NUMERICAL ANALYSIS OF FLOW FIELDS IN A SHELL AND TUBE HEAT EXCHANGER

by

Zhi-Yong YUE[a], Xiao-Xia YANG[b*], Yu-Jing ZHANG[a], Di-Xia PAN[a], and Chang XU[a]

[a] School of Mechanical Engineering, Inner Mongolia University of Technology, Hohhot, China
[b] Scientific Research Department, Inner Mongolia University of Technology, Hohhot, China

Original scientific paper
https://doi.org/10.2298/TSCI2303965Y

Shell and tube heat exchangers have great thermal stress due to the different fluid temperature and instability of the flow field. In this paper, based on the fluid physical model of shell and tube heat exchanger, the velocity field, pressure field and temperature field inside the heat exchanger are simulated and analyzed on Workbench platform. The numerical simulation shows that the baffle plate has a great influence on the internal flow field of the heat exchanger.

Key words: *shell and tube heat exchanger, ANSYS, the numerical simulation baffle plate*

Introduction

A shell-and-tube heat exchanger has the advantages in its wide application range, low production cost, easy manufacturing, simple structure, high reliability, strong processing capacity, wide range of materials, furthermore it can withstand high operating pressure and temperature [1-4]. The heat exchange efficiency through boundaries depends upon fluid property [5-7], and it was reported that nanofluids [4, 8, 9] can greatly enhance heat exchange.

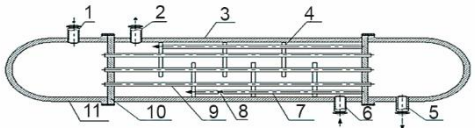

Figure 1. Structure diagram of the shell and tube heat exchanger; *1 – pipe flow inlet, 2 – shell side fluid inlet, 3 – shell, 4 – baffle, 5 – pipe flow outlet, 6 – shell side fluid outlet, 7 – spacer pipe, 8 – tie rod, 9 – heat exchange tube, 10 – tube sheet, and 11 – tube box*

The shell-and-tube heat exchanger consists of mainly shell, heat exchange tube, tube plate, baffle plate, tube box, pull rod and distance tube, *etc.* The shell is shaped like a cylinder, and there is a tube bundle composed of heat exchange tubes inside. The arrangement between the heat exchange tubes can be regular triangle, corner regular triangle and quadrilateral. In practice, the arrangement of heat exchange tubes used by enterprises is mostly regular triangle. The ends of the tube bundle are welded to the tube plate, and the tube plate is welded to the shell. There are two kinds of cold and hot fluids flowing in the heat exchanger. The flow in the heat exchange tube is called pipe side fluid, and the flow in the outside of the heat exchange is called the shell side fluid. The structure diagram of the shell-and-tube heat exchanger is illustrated in fig. 1. The flow fields (*e.g.* velocity distribu-

* Corresponding author, e-mail: 595607848@qq.com

tion, temperature distribution) in the shell and tube heat exchanger is very important for analyzing and improving the heat exchanger [10-14].

Numerical analysis of the shell and tube heat exchanger

Numerical methods are useful tool to analysis of a complex practical problems [15-19], this paper adopts the CFD. The governing equations include the continuity equation, the momentum conservation equations, and the energy conservation equation. The velocity, pressure, and temperature distributions can be numerically obtained. In this paper, the simulation domain is the inner basin of the shell-and-tube heat exchanger, the internal flow is complex, and some assumptions have to be made. The shell and tube side fluid flow and the heat transfer are steady, the shell side fluid is incompressible, and the thermal conductivity, viscosity and other physical parameters do not change in the simulation process, and there is no gap between the baffle plate and the heat exchange tube, the baffle plate and the inner wall of the shell, and there is no heat exchange between the outer wall of the shell and the outside world.

Common turbulence models include the direct numerical simulation (DNS), the large eddy simulation (LES), and the Raynaud time-homogeneous simulation (RANS) [20]. According to the number of differential equations, turbulence models can be divided into the zero-equation model, the single equation model, the two-equation model, the four-equation model, *etc.* The most commonly used two-equation model includes the standard k-ε model, the RNG k-ε model, the realizable k-ε model and k-ω model [21]. In this paper, the standard k-ε model [22], and FLUENT software [23] are adopted.

According to the actual operation of a polysilicon enterprise, the pipe side fluid is a high temperature fluid, the inlet temperature is about 470 ℃, the medium is hydrogen, chlorosilane exhaust gas and a small amount of silicon powder. The shell side fluid is a low temperature fluid, the inlet temperature is about 115 ℃, the medium is hydrogen and silicon tetrachloride. In order to reduce the amount of calculation in the process of computer simulation, the corresponding size of the original drawing is scaled in a certain proportion. At the same time, the inlet and outlet diameters of shell and shell are set as no wall thickness.

Table 1. Dimension table of each component

Name	Symbol	Size [mm]
Shell diameter	D_1	200
Length of heat exchange tube	L_1	1400
Outer diameter of heat exchange tube	D_o	25
Thickness of heat exchange tube	δ_1	2
Baffle thickness	δ_2	5
Baffle notch	h	50
Shell side inlet and outlet diameter	D_2	100

The total length of the simplified shell and tube heat exchanger is 1400 mm, the number of heat exchange tubes is 24, the heat exchange tubes are arranged in an equilateral triangle, and there are four arched baffles. The geometric parameters of each component of the heat exchanger are shown in tab. 1.

The simplified shell and tube heat exchanger is shown in fig. 2. The main structure is composed of shell, heat exchange tube and baffle.

The solid material of the heat exchange tube is S31608 (06Cr17Ni12Mo2) and is selected as the solid material of the baffle is s30408 (06cr19ni10). The shell has no wall thick-

ness, so there is no need to set the solid material of the shell. The physical parameters of relevant solid materials are shown in tab. 2 [24].

The tube side fluid of the shell and tube heat exchanger is hydrogen, chlorosilane and a small amount of silicon powder, the shell side fluid is hydrogen and silicon tetrachloride, and the tube side process is a parallel flow. The specific parameters are shown in tab. 3.

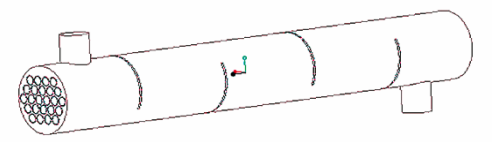

Figure 2. The 3-D model of shell and tube heat exchanger

Table 2. Physical parameters of each material

The digital code	The new brand	Density, ρ [kgdm^{-3}]	Specific heat, Cp [KJkg^{-1}K^{-1}]	Thermal conductivity, λ [Wm^{-1}K^{-1}]		Linear expansion coefficient, α [10^{-6}/K^{-1}]		Elastic modulus, E [Gpa]
				100 ℃	500 ℃	100 ℃	500 ℃	
S31608	06Cr17Ni12Mo2	8.00	0.50	16.3	21.5	16.0	18.5	193
S30408	06Cr19Ni10	7.93	0.50	16.3	21.5	17.2	18.4	193

Table 3. Determination of fluid parameters in tube and shell side

Name	The fluid passes	The shell side fluid
Thermal conductivity, λ [Wm^{-1}K^{-1}]	0.1014	0.2074
Viscosity, μ [Pa·s]	2.2786×10^{-5}	1.6185×10^{-5}
Specific heat at constant pressure, Cp [Jkg^{-1}K^{-1}]	7566	11130
Density, ρ [kgm^{-3}]	28.3671	36.0489
Inlet velocity, v [ms^{-1}]	5	4.5
Outlet velocity, t [℃] ?????	470	115
Outlet temperature, t [℃]	230	360

The unit sizes of the shell side fluid domain, the tube side fluid domain, the baffle, and the heat exchange tube are 5 mm, 4 mm, 4 mm, and 3 mm, respectively. The hybrid grid dominated by hexahedron is divided. After division, the number of grids is more than 1.1 million and the number of nodes is 5.88 million, as shown in fig. 3.

Boundary conditions meet the mathematical and physical requirements. A unique solution can be obtained for given initial conditions and boundary conditions. Setting boundary conditions is a key step in numerical simulation, which will affect the simulation accuracy and convergence rate [25], and this paper ignores the fluid-solid interaction [26]. This paper considers only smooth boundary, though unsmooth boundary affects greatly the flow properties, for example, the unsmooth boundary will greatly affect the solitary wave travelling [27-29], a porous surface has a special thermal and mechanical properties [30, 31], the fractal boundary of a desert has less friction [32].

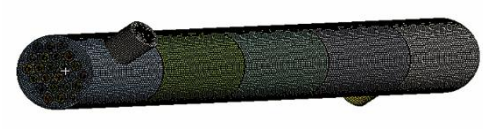

Figure 3. Mesh division of the shell and tube heat exchanger

The inlet of the tube and shell side is given the velocity boundary condition. The velocity of the tube side is set as 5 m/s, the inlet temperature is set as 470 ℃, the inlet velocity is set as 4.5 m/s, and the inlet temperature is set as 115 ℃. The outlet of the tube and shell side is given the pressure boundary condition and the static pressure at the outlet of the tube and shell side is set as 0 Pa.

The solution methods are as shown in tab. 3. Leave the relaxation factor as default and then initialize it. Run computationally iterated steps to 500, change the residual in continuity in residual monitors to 0.0001, and set the rest to default. Finally, click calculate for iterative calculation.

Table 3. Choice of solution method

Name	Method
Pressure-velocity coupling	Simple
Pressure	Second order
Momentum	Second order upwind
Turbulent kinetic energy	First order upwind
Turbulent dissipation rate	First order upwind
Energy	Second order upwind

Analysis of numerical simulation results of shell and tube heat exchanger

Through the FLUENT module simulation, the distribution of the velocity field, pressure field and temperature field of the fluid in the tube and shell side are obtained.

Analysis of the velocity field

As shown in fig. 4, the shell-side fluid enters at the inlet at a speed of 4.5 m/s. The presence of the bow-shaped baffle makes the shell-side fluid's velocity present a *Z*-shaped periodic change. When the fluid-flows through the baffle gap, the velocity sees a sudden change, the velocity value of the location in this area is relatively large and the direction changes, the maximum flow velocity reaches 11 m/s. The sudden change in flow velocity at the gap of the baffle will impact the heat exchange tubes nearby, and the heat exchange tubes with compact structure will vibrate, causing damage to the heat exchange tubes. The sudden change in the velocity of the shell side fluid at the baffle will impact the baffle and cause the baffle to deform, and it can also cause collision between the baffle and the heat exchange tube.

In the shell-side channel, the static area of the shell-side flow velocity and the area of the shell-side fluid stagnation are called the dead zone of flow. As shown in figs. 4 and 5, the blue area is on the back of the baffle, the fluid velocity is very small, about 0.3 m/s, and the direction of the fluid is vortex on the back of the baffle, indicating that the baffle is an obvious flow dead zone on the back, and the fluid collected on the back of the baffle cannot effectively transfer heat through the gap of the baffle, which affects the temperature of the shell side exit and causes the heat exchange capacity of the shell-and-tube heat exchanger to decrease.

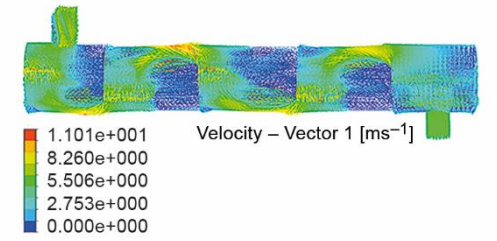

Figure 4. Velocity vector diagram of shell side fluid

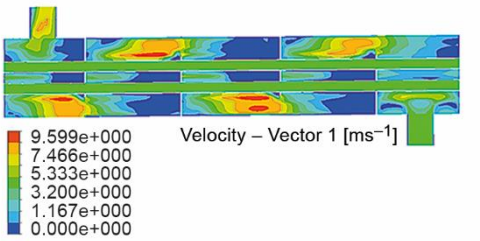

Figure 5. Velocity cloud diagram of *Y-Z* section with *X* = 0

As shown in fig. 5, when the *X-Z* section is made at the entrance, the speed at the entrance of the same section is relatively large, and there is an obvious sudden change in speed near the heat exchange tube, which will cause erosion and damage to the heat exchange tube at the entrance. In turn, it will cause erosion damage to the anti-scouring board. From fig. 6, it can be seen that when the fluid flows at the inlet, there will be a vortex, which continuously impacts the tube sheet.

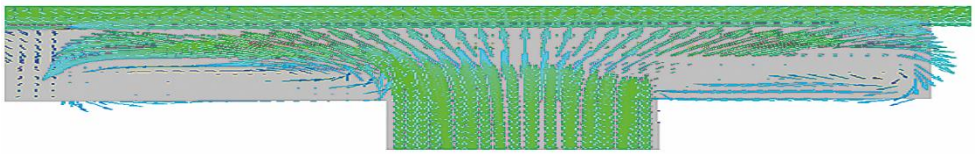

Figure 6. Enlarged view of velocity vector at entrance of *Y-Z* section with *X* = 0

Select six points in the velocity cloud diagram of the *Y-Z* section, points 1~3 are located at the entrance, Points 4~6 at the exit, Point 1 and Point 4 are the lower part of the shell path, Point 2 and Point 5 is the middle part of the shell side, and Points 3 and 6 are the upper part of the shell side. The velocity values of each point of the shell side fluid are shown in tab. 4.

Table 4. Velocity value of each point

Points at the entrance [m]	Velocity [ms^{-1}]	Points at the exit [m]	Velocity [ms^{-1}]
Point 1 (0, 0.58, 0.06)	5.08	Point 4 (0, –0.58, 0.06)	7.02
Point 2 (0, 0.58, 0)	1.67	Point 5 (0, –0.58, 0)	3.36
Point 3 (0, 0.58, –0.06)	2.38	Point 6 (0, –0.58, –0.06)	4.91

It can be seen from the above table that the flow velocity near the two sides of the shell is greater than the flow velocity in the middle of the shell, indicating that the heat exchanger tubes near the two sides of the shell are more vulnerable to be damaged than the heat exchange tubes in the middle part, this is mainly caused by the bow baffle. According to the previous analysis, the structure of the arcuate baffle will have a certain impact on the operation of the shell-and-tube heat exchanger and cause the failure of the heat exchanger.

For the tube side fluid, the inlet velocity is 5 m/s. It can be seen from figs 4-6 that the velocity does not change much in the heat exchange tube, and heat is exchanged in a basic way, so the velocity has little effect on the failure of the heat exchanger.

Analysis of is pressure field

In order to observe the change of fluid pressure field intuitively, we take the *Y*-*Z* cross-section with $X = 0$ for analysis, the pressure cloud diagram of the *Y*-*Z* section is shown in fig. 7.

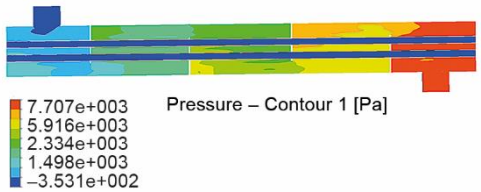

Figure 7. Pressure cloud diagram of *Y*-*Z* section with $X = 0$

In order to observe the pressure distribution clearly, we take the six positions at the entrance, the gaps of the four baffles, and the exit to measure the pressure values. The pressure values at each position are shown in tab. 5.

Table 5. Pressure value of each point

Position of each point [m]	Pressure [Pa]	Position of each point [m]	Pressure [Pa]
Entrance (0, 0.58, 0.15)	7339.96	First baffle (0, 0.45, –0.065)	6102.68
Second baffle (0, 0.15, 0.065)	4654.40	Third baffle (0, –0.15, –0.065)	2863.45
Fourth baffle (0, –0.45, 0.065)	1354.82	Exit (0, –0.58, –0.15)	–71.91

Next, we analyze the *X*-*Z* section with $Y = 0$, that is, the pressure field changes at the side positions of the second baffle and the third baffle. The pressure cloud diagram of the *X*-*Z* section is shown in fig. 8.

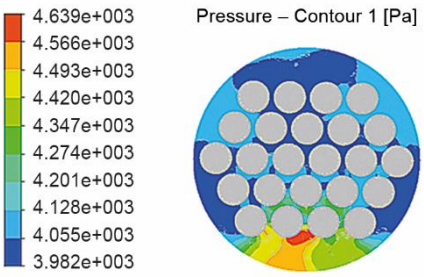

Figure 8. Pressure cloud diagram of *X*-*Z* section with $Y = 0$

From fig. 7 and tab. 5, it can be seen intuitively that the pressure is the largest near the inlet of the shell side, reaching 7329.96 Pa. The pressure will be significantly reduced when the fluid flows through each baffle, and the pressure gradient is high. The pressure near the entrance is the smallest at –71.91 Pa, and the pressure drop at the entrance and exit is 7411.87 Pa. Similar to the analysis of the velocity field, the shell-side fluid also has a sudden pressure change at the baffle. This is because the fluids rub and collide with each other in the flow. The vortex and backflow of the fluid cause continuous loss of energy. This pressure drop will damage the heat exchange tube and the baffle at the gap of the baffle. This is because at the second baffle and the third baffle, the fluid flows from the lower side of the shell to the upper side, and there is a phenomenon of circumfluence and detachment. This phenomenon produces energy consumption, resulting in obvious pressure drop.

Analysis of temperature field

Analysis of the fluid temperature field in the shell side of the tube

Figure 9 shows the temperature cloud diagram of the shell-side fluid at the *Y-Z* section where $X = 0$. It can be seen from the figure that the temperature of the shell-side fluid passing through the cross-flow path is continuously increasing, and the temperature will undergo a sudden change when it passes through each baffle, which shows that the function of the baffle is to enhance heat transfer and extend the heat transfer time, and at the same time, the temperature change of the fluid in the shell side will directly affect the temperature change of the solid region of the heat exchanger. The temperature change at the position, where the heat transfer dead zone appears on the back of the baffle, is obvious. This is because the velocity in the heat transfer dead zone is very low, and the fluid circulates nearby, the average temperature of the tube side fluid is 427 °C and the temperature of the shell side fluid in the heat transfer dead zone becomes higher through heat transfer. The temperature at the entrance of the shell side is 115 °C, and the temperature measured at the exit is 193.95 °C, which is in line with the heat exchange law of the heat exchanger, but the temperature difference between the entrance and exit is 78.95 °C, which is a certain difference from the expected temperature, indicating that the heat transfer capacity is reduced.

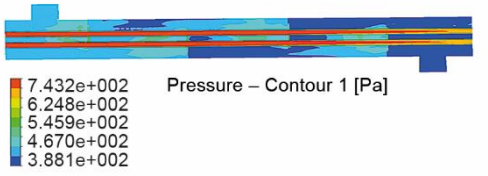

Figure 9. Temperature cloud diagram of *Y-Z* section with $X = 0$

For the tube side fluid, it is observed from the figure that the tube side entrance temperature is 470 °C. As the heat exchange time increases, the tube side fluid has a temperature difference in its axial direction, the outlet temperature is 384.15 °C, which is consistent with the heat exchange regularity of the heat exchanger, however, the temperature difference between the inlet and outlet is 85.85 °C, which is different from the expected temperature, indicating that the heat transfer capacity is reduced because of the dead zone and backflow of the shell side fluid. The coincidence of temperature analysis and shell-side fluid velocity analysis also further demonstrates the correctness of the numerical simulation.

Analysis of temperature field in solid domain

Figure 10 is the temperature cloud diagram of the tube and the shell. It can be seen from the figure that the temperature difference between the heat exchange tube bundle and the shell is about 290 °C. The temperature difference between the tube and the shell will cause the heat exchanger to generate a thermal stress, which will damage the heat exchange tube and the shell. It can be seen from fig. 11 that the maximum temperature of the heat exchange tube occurs in the baffle area, which will cause the heat exchange tube near the baffle to deform.

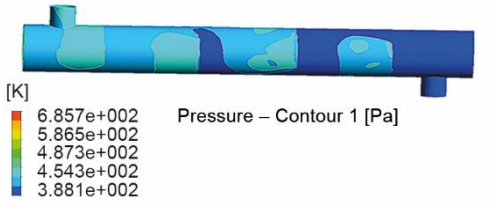

Figure 10. Temperature cloud diagram of solid region of shell and tube heat exchanger

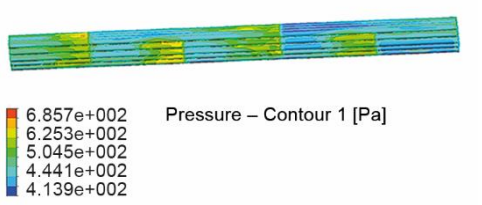

Figure 11. Temperature cloud diagram of heat exchange tube

Conclusion

The velocity, pressure and temperature distributions of the heat exchanger are obtained by ANSYS Workbench platform. It is observed in the velocity vector diagrams and cloud diagrams that the shell side fluid changes in a *Z*-shape, and the velocity is relatively large at the baffle hole. The heat exchange tube near the shell is more likely to be damaged, and there is an obvious flow dead zone on the back of the baffle plate, which affects the heat transfer efficiency. It is observed from the pressure cloud chart that the pressure is the largest near the inlet of the shell side and the smallest near the outlet. The pressure decreases obviously after passing through a baffle plate, and the pressure drop of the inlet and outlet reaches 7411.87 Pa. It is observed from the temperature cloud that the temperature at the back of the baffle plate is relatively high, which is caused by the heat transfer dead zone. The temperature difference between the shell and the heat exchange tube bundle is about 290 °C, which will produce thermal stress and cause damage to the heat exchange tube and the shell.

References

[1] Emilio, D. B., *et al.*, Modeling and Prediction of Shell-Side Fouling in Shell-and-Tube Heat Exchangers, *Heat Transfer Engineering, 40* (2019), 11, pp. 845-861
[2] Bozorgan, N., *et al.*, Design and Thermal-hydraulic optimization of a shell and tube heat exchanger using bees algorithm, *Thermal Science, 26* (2022), 1B, pp. 693-703
[3] Aydin, A., *et al.*, Optimization and CFD analysis of a shell-and-tube heat exchanger with a multi segmental baffle, *Thermal Science, 26* (2022), 1A, pp. 1-12
[4] Sajjad, M., *et al.* Thermal-Hydraulic Analysis of Water Based ZrO_2 Nanofluid in Segmental Baffled Shell and Tube Heat Exchangers, *Thermal Science, 24* (2020), 2B, pp. 1195-1205
[5] He, J.H., *et al.*, Non-linear EHD Instability of Two-Superposed Walters' B Fluids Moving through Porous Media, *Axioms, 10* (2021), 4, 258
[6] He, J. H., Mostapha, D. R., Insight into the Significance of Hall Current and Joule Heating on the Dynamics of Darcy-Forchheimer Peristaltic Flow of Rabinowitsch Fluid, *Journal of Mathematics, 2021* (2021), Oct., 3638807
[7] He, J. H., *et al.*, Non-linear Instability of Two Streaming-Superposed Magnetic Reiner-Rivlin Fluids by He-Laplace Method, *Journal of Electroanalytical Chemistry, 895* (2021), Aug., 115388
[8] Eldabe, N. T., *et al.*, Effect of Induced Magnetic Field on Non-Newtonian Nanofluid Al_2O_3 Motion Through Boundary-Layer with Gyrotactic Microorganisms, *Thermal Science, 26* (2022), 1B, pp. 411-422
[9] He, J. H., Abd-Elazem, N. Y., Insights into Partial Slips and Temperature Jumps of a Nanofluid Flow over a Stretched or Shrinking Surface, *Energies, 14* (2021), 20, 6691
[10] Abdulrahman, R. S., *et al.*, Numerical Study of Heat Transfer and Exergy Analysis of Shell and Double Tube Heat Exchanger, *International Journal of Heat and Technology, 38* (2020), 4, pp. 925-932
[11] Koorosh, M., *et al.*, Numerical Investigation of the Effect of Baffle Orientation on Heat Transfer and Pressure Drop in a heat exchanger With Leakage Flows, *Heat Transfer Engineering, 30* (2009), 14, pp. 1123-1135

[12] Ko, J. H., *et al.*, Development of a Low Reynolds Number Enhanced Heat Transfer Surface Using Flow Visualization Techniques, *International Journal of Heat and Fluid Flow, 23* (2002), 4, pp. 444-454
[13] Ambekar, A. S., *et al.*, CFD Simulation Study of Heat Exchangers with Different Baffle Segment Configurations, *Applied Thermal Engineering, 108* (2016), Sept., pp. 999-1007
[14] Rossetti, A., *et al.*, A Simplified Thermal CFD Approach to Fins and Tube Heat Exchanger: Application to Maldistributed Airflow on an Open Display Cabinet, *International Journal of Refrigeration, 57* (2015), Sept., pp. 208-215
[15] Wang, C. C., Yau, H. T., Application of a Hybrid Numerical Method to the Bifurcation Analysis of a Rigid Rotor Supported by a Spherical Gas Journal Bearing System, *Non-linear Dynamics, 51* (2008), 4, pp. 515-528
[16] Chen, C. L., *et al.*, Performance Analysis and Optimization of a Solar Powered Stirling Engine with Heat Transfer Considerations, *Energies, 5* (2012), 9, pp. 3573-3585
[17] Yuan, H., *et al.*, Numerical Study on the Flow and Heat Transfer of Water-Based $A1_2O_3$ Forced Pulsating Nanofluids Based on Self-Excited Oscillation Chamber Structure, *Thermal Science, 26* (2022), 1B, pp. 489-501
[18] Yu, W., *et al.*, Tensorizing GAN with High-Order Pooling for Alzheimer's Disease Assessment, *IEEE Transactions on Neural Networks and Learning Systems, 33* (2021), 9, pp. 4945-4959
[19] Hu, S., *et al.*, Bidirectional Mapping Generative Adversarial Networks for Brain MR to PET Synthesis, *IEEE Transactions on Medical Imaging, 41* (2021), 1, pp. 145-157
[20] Xu, W. C., Jun, H., *Computational Fluid Dynamics*, Beijing Institute of Technology Press (in Chinese), Beijing, 2011, pp. 38-40
[21] Lu, L., *et al.*, Turbulence Models Assessment for Separated in a Rectangular Asymmetric Three-Dimensional Differ, *Engineering Computations, 33* (2016), 4, pp. 978-994
[22] Ding, X. S., *et al.*, *FLUENT 14.5 Fluid Simulation Calculations from Begin to Master* (in Chinese), Beijing, Tsinghua University Press, Beijing, 2014:116-120
[23] Chamil A. Compact Heat Exchangers-Design and Optimization with CFD, *International Journal of Heat and Mass Transfer, 146* (2020), Jan., pp. 1-13
[24] Zeng, Z. M., *Practical metal materials selection Manual* (in Chinese), Beijing: China Machine Press, 2012, pp. 191-193
[25] Cai, H. W., *Heat Stress Analysis and Structure Optimization of Fixed Tube-plate Heat exchanger* (in Chinese), Nanchang University, Nanchang, China, 2018
[26] Chen, C.L., *et al.*, Terminal Sliding Mode Control for Aeroelastic Systems, *Non-linear Dynamics, 70* (2012), 3, pp. 2015-2026
[27] He, J. H., *et al.*, Variational Approach to Fractal Solitary Waves, *Fractals, 29* (2021), 7, 2150199
[28] He, J. H., *et al.*, Solitary waves Travelling Along an Unsmooth Boundary, *Results in Physics, 24* (2021), May, 104104
[29] Wu, P. X., *et al.*, Solitary Waves of the Variant Boussinesq-Nurgers Equation in a Fractal Dimensional Space, *Fractals, 30* (2022), 3, pp. 1-10
[30] He, C. H., *et al.*, A Fractal Model for the Internal Temperature Response of a Porous Concrete, *Applied and Computational Mathematics, 21* (2022), 1, pp. 71-77
[31] He, C. H., *et al.*, A Novel Bond Stress-Slip Model for 3-D Printed Concretes, *Discrete and Continuous dynamical Systems, 15* 2022), 7, pp. 1669-1683
[32] Mei, Y., *et al.* On the Mountain-River-Desert Relation, *Thermal Science, 25* (2021), 6B, pp. 4817-4822

Paper submitted: December 19, 2021
Paper revised: March 20, 2022
Paper accepted: March 20, 2022